Received: 22 November 2023 | Revised: 25 March 2024 | Accepted: 27 March 2024

DOI: 10.1002/ar.25451

SPECIAL ISSUE ARTICLE

The Anatomical Record WILEY

Comparing cranial biomechanics between *Barbourofelis fricki* and *Smilodon fatalis*: Is there a universal killing-bite among saber-toothed predators?

Borja Figueirido[1] | **Shane Tucker**[2] | **Stephan Lautenschlager**[3,4]

[1]Departamento de Ecología y Geología, Facultad de Ciencias, Universidad de Málaga, Málaga, Spain

[2]Department of Earth and Planetary Sciences, University of Nebraska State Museum, Lincoln, Nebraska, USA

[3]School of Geography, Earth and Environmental Sciences, University of Birmingham, Birmingham, UK

[4]The Lapworth Museum of Geology, Birmingham, UK

Correspondence
Borja Figueirido, Departamento de Ecología y Geología, Facultad de Ciencias, Universidad de Málaga, Campus de Teatinos s/n, 29071 Málaga, Spain.
Email: borja.figueirido@uma.es

Funding information
Junta de Andalucía, Grant/Award Numbers: P18-FR-3193, UMA18-FEDERJA-188; Ministerio de Ciencia, Innovación y Universidades; Ministerio de Economía y Competitividad, Grant/Award Numbers: CGL2015-68300P, PID2019-111185GB-I00

Abstract

Saber-tooths, extinct apex predators with long and blade-like upper canines, have appeared iteratively at least five times in the evolutionary history of vertebrates. Although saber-tooths exhibit a relatively diverse range of morphologies, it is widely accepted that all killed their prey using the same predatory behavior. In this study, we CT-scanned the skull of *Barbourofelis fricki* and compared its cranial mechanics using finite element analysis (FEA) with that of *Smilodon fatalis*. Our aim was to investigate potential variations in killing behavior between two dirk-toothed sabretooths from the Miocene and Pleistocene of North America. The study revealed that *B. fricki* had a stoutly-built skull capable of withstanding stress in various prey-killing scenarios, while the skull of *S. fatalis* appeared less optimized for supporting stress, which highlights the highly derived saber-tooth morphology of the former. The results may indicate that *B. fricki* was more of a generalist in prey-killing compared to *S. fatalis*, which experiences lower stresses under stabbing loads. We hypothesize that morphological specialization in saber-tooths does not necessarily indicate ecological specialization. Our results support the notion that morphological convergence among saber-toothed cats may obscure differences in hunting strategies employed to dispatch their prey. Our findings challenge the assumption of the universally assumed canine-shear biting as the prey-killing behavior of all saber-toothed cats. However, further research involving a wider range of dirk and scimitar-toothed forms could provide additional insights into the diversity of cranial biomechanics within this fascinating group of extinct mammalian predators.

KEYWORDS

Barbourofelis, finite element analysis, predatory behavior, skull, *Smilodon*

1 | INTRODUCTION

Saber-tooths extinct apex predators with elongate and blade-like (mediolaterally compressed) upper canines that have attracted much interest from both scientists and the public alike. Saber-tooths have appeared iteratively at least five times in the evolutionary history of vertebrates (Van Valkenburgh, 2007; Lautenschlager et al., 2020): in non-mammalian synapsids (Permian gorgonopsians) and, within mammals, in both metatherians (the Plio-Pleistocene South American sparassodont [Mammalia, Sparassadonta, Thylacosmilidae] *Thylacosmilus atrox*), and eutherians (the oxyaenids [Mammalia, Oxyaenida] of the genus *Machaeorides* and *Apataelurus*, the Miocene Nimravidae [Mammalia, Carnivora], and in machairodont felids [Mammalia, Carnivora, Felidae]). In all these forms, and more specifically in placentals, their canine morphology contrasts with the conical-shaped canines of living felines and provides valuable insights into the ecological niche occupied by these formidable predators (Faith et al., 2018; Van Valkenburgh et al., 2016). Indeed, it is widely assumed that the saber-tooth morphology probably represents an adaptation to accommodate these iconic teeth and kill 'megaherbivore' prey (e.g., Bohlin, 1940; Emerson & Radinsky, 1980; Simpson, 1941).

To kill large herbivores, saber-tooths necessarily had to maximize jaw gape up to 120° for canine clearance and, therefore, around 30° more than living conical-toothed cats (Andersson et al., 2011). However, jaw gape maximization led to a major reorganization of their craniodental morphology aimed at minimizing strain on muscles during wide gaping actions, including: (i) a verticalization of the temporalis fossa with a shorter coronoid process, leading to longer temporalis fibers, which would have allowed greater muscle extension and thereby a wider gape; (ii) a descended glenoid fossa, allowing for more force in head strikes through an optimized moment arm provided by certain neck muscles; (iii) an enlarged mastoid process, reflecting enlarged neck muscles (i.e., sternomastoid, obliquus capitis cranialis) and indicating a greater moment arm for head depressors; (iv) a lanceolate-shaped occiput, to further enhance the moment arm of head-elevator muscles and maximize its effectiveness on head-strike motions; and (v) an upwardly rotated face with a higher attachment of the upper canines (Emerson & Radinsky, 1980; Kurtén, 1952; Matthew, 1910). However, the presence of a short coronoid process indicates less leverage for the temporalis and, therefore, less force at the carnassial and canines (Emerson & Radinsky, 1980; Figueirido et al., 2011; Matthew, 1910; McHenry et al., 2007; Simpson, 1941), making it unlikely that the mandibular adductors could generate enough force to use a suffocating throat bite as living conical-toothed cats regularly do (Turner et al., 2011). Accordingly, previous researchers have proposed a shift in their jaw mechanics; unlike present-day pantherine cats, saber-tooths adopted a neck-powered biting strategy with a pivot point located behind the head (e.g., Akersten, 1985; Antón & Galobart, 1999; Bryant, 1996; Matthew, 1910; Simpson, 1941) and this reorganization allowed neck muscles to drive the bite in a head nodding motion (e.g., Antón et al., 2004; Antón & Galobart, 1999; Ballesio, 1963; Schaub, 1925). Moreover, other biomechanical studies of the skull based on finite element analysis (FEA) have supported the neck-powered biting hypothesis (e.g., Figueirido et al., 2018; McHenry et al., 2007; Wroe et al., 2013).

Strikingly, despite the dramatic reorganization of their craniomandibular skeleton, saber-tooths have appeared iteratively across various times and ecosystems. Therefore, it is not surprising that despite their first-order similarities derived from the necessity to maximize jaw gape for canine clearance mentioned above, there are second-order differences that have given rise to a relatively diverse range of morphologies (e.g., Martin, 1980; Slater & Van Valkenburgh, 2008). For instance, the degree of the elongation and width of the canine, the development of the coronoid, mental and mastoid processes, the appearance of serrations in the blades of canines and carnassials, and the appearance of a well-developed postorbital bar (Emerson & Radinsky, 1980). However, despite this remarkable phenotypic variability of saber-tooths (Emerson & Radinsky, 1980), it was widely accepted that all killed their prey using the same predatory behavior.

Various speculations and hypotheses regarding the killing behavior of saber-tooths have been proposed, such as neck-flexing stabbing (Matthew, 1910), dynamic-stabbing (Simpson, 1941), slicing (Bohlin, 1940), shear-biting (Akersten, 1985) and a forelimb-powered lever model (Brown, 2014). Among them, the canine-shear bite model proposed by Akersten (1985) has gained significant support and acceptance among researchers, which proposes that saber-tooths supplemented the jaw-closing force of its mandibular adductors with a ventral depression of the head to deliver a precise and powerful killing bite onto the belly of prey (Akersten, 1985) or, as later proposed by Antón and Galobart (1999), onto the throat where there is an increased chance of major blood vessels injury.

In recent years, there has been a growing body of research focused on understanding the morphological disparity among different saber-tooth species and its relationship to their killing behavior (e.g., Chatar et al., 2022; Gaillard et al., 2023; Janis et al., 2020; Lautenschlager et al., 2020; Melchionna et al., 2021; Piras et al., 2013; Wroe et al., 2013). Recent research has highlighted the complexity and diversity of saber-tooth killing behavior,

challenging previous assumptions, and shedding light on the morphofunctional disparity within this group of formidable predators (e.g., Chatar et al., 2022; Lautenschlager et al., 2020). However, in the early eighties, it was proposed that there were two distinct ecomorphs within saber-tooths based on craniodental and postcranial morphology (Martin, 1980). The first ecomorph is known as the "scimitar-tooth", which includes species like *Homotherium* or *Amphimachairodus*. These forms have shorter canines with coarsely serrated margins and a more gracile skeleton, indicating a cursorial predatory behavior. The second ecomorph is called the "dirk-tooth", which includes species such as *Smilodon* or *Megantereon*. Dirk-toothed forms have longer canines with moderate lateral compression and fine serrations (or no serrations), coupled with a stout appendicular skeleton, which suggests a super-ambush predatory behavior. Recent research using three-dimensional computer simulations using finite element analysis has further demonstrated variations in predatory behavior between *Smilodon fatalis* and *Homotherium serum*—two highly derived dirk- and scimitar-toothed forms from the Pleistocene of North America (Figueirido et al., 2018). Indeed, Figueirido et al. (2018) demonstrated that *Smilodon* was adapted to deliver a quick stabbing bite to the prey's throat, while *Homotherium* likely used debilitating slashing bites to subdue large prey. These findings support previous functional analyses of saber-tooth craniodental morphology (e.g., Therrien, 2005), highlighting the diversity of potential feeding behaviors and killing strategies employed by different species, which raises questions about the generalization of their killing behavior.

Interestingly, there are significant morphological differences among different species of saber-tooths. This is true not only between scimitar and dirk-toothed forms but also among species within the same ecomorph. For instance, the cat-like *Barbourofelis fricki* (Nimravidae; Barbourofelinae [Barrett, 2021; Barrett et al., 2021; Wang et al., 2020]) and the machairodont *Smilodon fatalis*, two highly specialized dirk-tooths from the late Miocene and Pleistocene of North America, respectively, exhibit profound morphological differences (Figure 1). However, whether these morphological differences impact functional performance and so indicate potential variations in killing behavior among species within the same ecomorph remains unknown. This is surprising because while *S. fatalis* is the quintessential example of a saber-tooth, *B. fricki* exhibits more derived traits towards the sabertoothed ecomorph (Figure 1), but the latter has been understudied from a biomechanical point of view.

In this study, we compare the cranial mechanics of *B. fricki* and *S. fatalis* using finite element analyses from CT-scanned skulls to make inferences about their killing

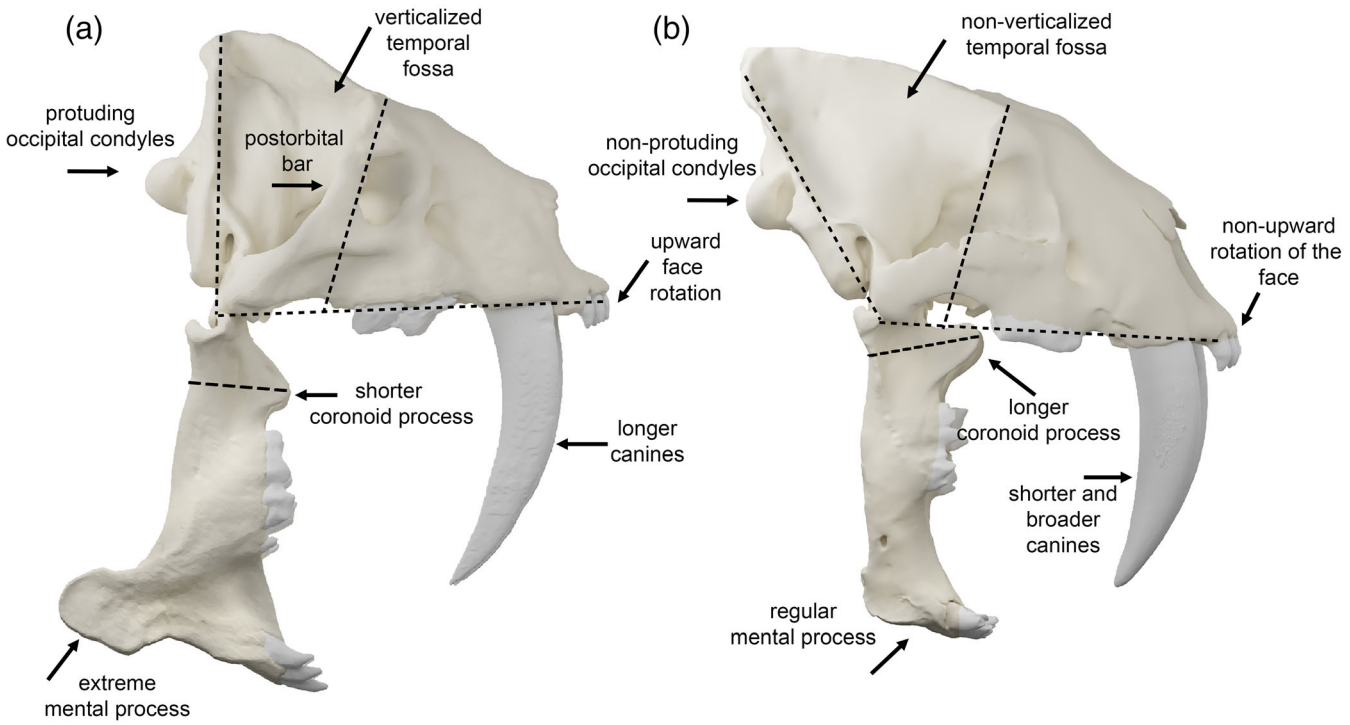

FIGURE 1 Morphological differences between *B. fricki* (a) and *S. fatalis* (b). The skulls are scaled to same length from prostion to basion.

behavior. Our main goal is to investigate whether the morphological differences in the skull between these two taxa are also related to differences in their cranial mechanics. Our findings confirm this assumption, indicating variations in the killing behavior between species within the same ecomorph, a result that casts doubts about the generalization of the saber-tooth killing repertoire even for species allocated within the same ecomorph.

2 | MATERIALS AND METHODS

2.1 | CT-scanning of fossil skulls

The crania of the two extinct saber-tooths, *B. fricki* (UNSM 76000) and *S. fatalis* (LACMRLP R37376) were CT scanned. Both specimens were adults as indicated by fully closed synchondroses and complete tooth eruption. The skull of *S. fatalis* was scanned at the University of Texas High-Resolution X-ray Computed Tomography Facility and the scan is available on the UT Digital Morphology website (http://www.digimorph.org/). The acquisition properties for *S. fatalis* were 1024 × 1024 16-bit TIFF images, 420 kV, 1.8 mA, with voxel size in mm of 0.2143 (*X*), 0.2143 (*Y*), 0.5000 (*Z*) (total slices = 629). The specimen of *S. fatalis* (LACMRLP R37376) is from Rancho La Brea (Los Angeles, California) collected at Pit 91.

The skull of *B. fricki* was scanned at Advanced Medical Imaging in Lincoln (Nebraska, USA) using a medical CT-scanner GE LightSpeed VCT using three different CT-scans for the skull, mandible and upper canines. The acquisition properties for *B. fricki* were: (i) for the skull 512 × 512 16-bit DICOM images, 120 kV, 100 mA, with voxel size in mm of 0.5019530 (*X*), 0.5019530 (*Y*), 0.625 (*Z*) (total slices = 485); (ii) for the jaw 512 × 512 16-bit DICOM images, 120 kV, 100 mA, with voxel size in mm of 0.5058590 (*X*), 0.5058590 (*Y*), 0.625 (*Z*) (total slices = 521); (iii) for the canines 512 × 512 16-bit DICOM images, 120 kV, 100 mA, with voxel size in mm of 0.5156250 (*X*), 0.5156250 (*Y*), 0.625 (*Z*) (total slices = 460).

The CT data was processed using Avizo (version 8, Visualization Science Group). As the fossil material is well preserved and relatively-free of matrix, segmentation could be performed using the automatic thresholding tool in Avizo's Segmentation Editor; only the teeth required manual segmentation using the paintbrush tool. In addition, minor preservational artifacts, including small fractures and breaks, were removed during the segmentation process following the protocols outlined in Lautenschlager (2016). Moreover, the distal third of the upper canines were reconstructed in the original holotype of *B. fricki* and this reconstruction was retained for the digital models. Similarly, in the case of *S. fatalis*, the tips of the canines were also reconstructed as in Figueirido et al. (2018).

For the subsequent generation of the biomechanical models, the three CT scans were combined using the 3D modeling software Blender (version 3.2, www.blender.org). The isolated upper canine teeth were fitted into the alveoli in the skull. Remnants of the original canine roots revealed by the CT scans were used as a guide to scale the isolated teeth to their correct size. The mandible was placed in its corresponding position articulating with the skull at the jaw joint.

2.2 | Volumetric muscle reconstruction

The jaw adductor musculature for both species was reconstructed to provide realistic input parameters for the subsequent biomechanical analyses. The methodology is described in detail in and largely follows Lautenschlager (2013) and Herbst et al. (2022). Muscle attachment sites on the digital skull and mandible models were identified for each jaw adductor muscle independently, based on osteological correlates such as muscle scars, ridges, and depressions (Figures 2 and 3). To connect the origin and insertion sites and flesh out the muscles, we used 'MyoGenerator', a Blender add-on for volumetric muscle construction (Herbst et al., 2022). This approach creates adjustable muscle curves by making NURBS (non-uniform rational B-splines) paths connecting the centroids of the origin and insertion sites. Following this semi-automatic generation of the three-dimensional muscle bodies, the final adjustments were made using the in-built sculpting tools in Blender to remove any intersections between muscles or between muscles and bone. Six jaw adductor muscles were reconstructed for each species using this method: m. temporalis pars superficialis, m. temporalis pars profunda, m. masseter pars superficialis, m. masseter pars profunda, m. pterygoideus pars interna, m. pterygoideus pars externa (Figures 2 and 3). For the muscle reconstruction, the mandible was rotated into a fully closed position, assuming maximum muscle contraction at a closed gape angle.

Muscle forces for each individual muscle were calculated using the "dry skull" method by multiplying the muscle cross-section area (CSA) by an isometric muscle stress of 0.3 N/mm^2 (Thomason, 1991). The CSA was calculated by dividing muscle volume (MV) by muscle length (ML). Both values (MV, ML) were obtained from the 'MyoGenerator' output.

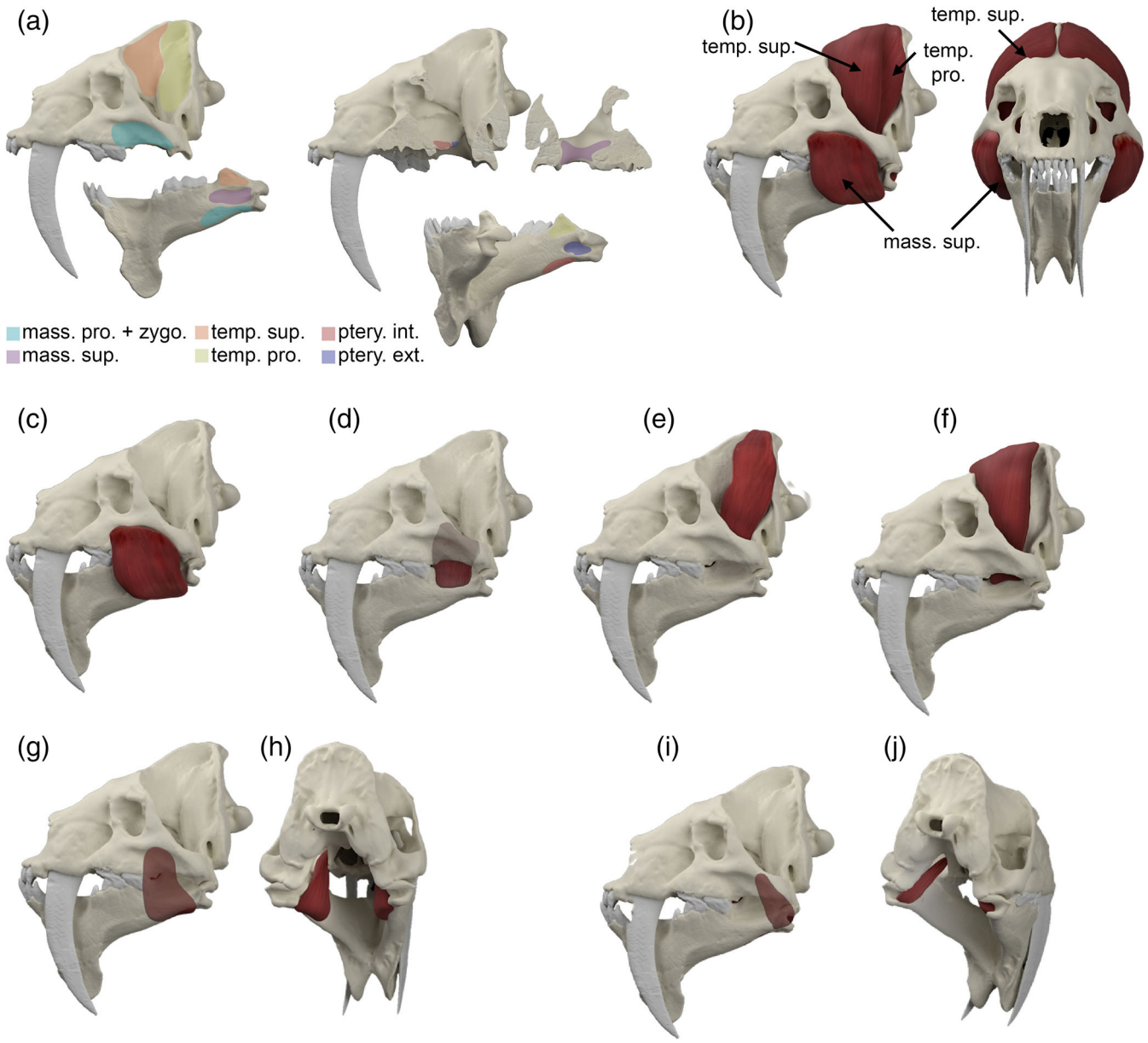

FIGURE 2 Origin and insertion areas for *B. fricki* based on muscle scars and topological criteria for the three-dimensional muscle reconstruction. (a) Origin and insertion areas of main masticatory muscles reconstructed for intrinsic scenarios. (b) Reconstruction of temporalis pars supficialis and pars profunda as well as the masseter pars superficialis. (c) The masseter pars superficialis. (d) Masseter pars profunda. (e) Temporalis pars profunda. (f) Temporalis pars superficialis. (g) and (h) Pterygoid pars interna in different views. (i) and (j) Pterygoid pars externa in different views. mass. pro., masseter pars profunda; mass. sup., masseter pars superficialis; temp. pro., temporalis pars profunda; temp. sup., temporalis pars superficialis; ptery. int., pterigoyd pars interna; ptery. ext., pterygoid pars externa.

2.3 | Gape analyses

The digital models of the cranium and mandible of *B. fricki* and *S. fatalis* were imported into Blender for muscle-constrained gape angle analyses following Lautenschlager (2015). The separate cranium and mandible models were connected using an armature (Blender's animation tool) with a center of rotation at the jaw joint. The jaw adductor muscles were modeled as simple cylinders connecting the corresponding origin and insertion sites. The cylinders were connected to the armature, allowing them to extend as the mandible rotated. A Python script was used to measure the tension of each muscle cylinder throughout the modeled jaw opening cycle. A maximum tension limit of 170% of the resting length was assumed (Nigg & Herzog, 2007; Sherwood et al., 2012). This structural constraint was used by Lautenschlager (2015) to estimate the maximum gape angle at which the limit of maximum tension is reached. In the case

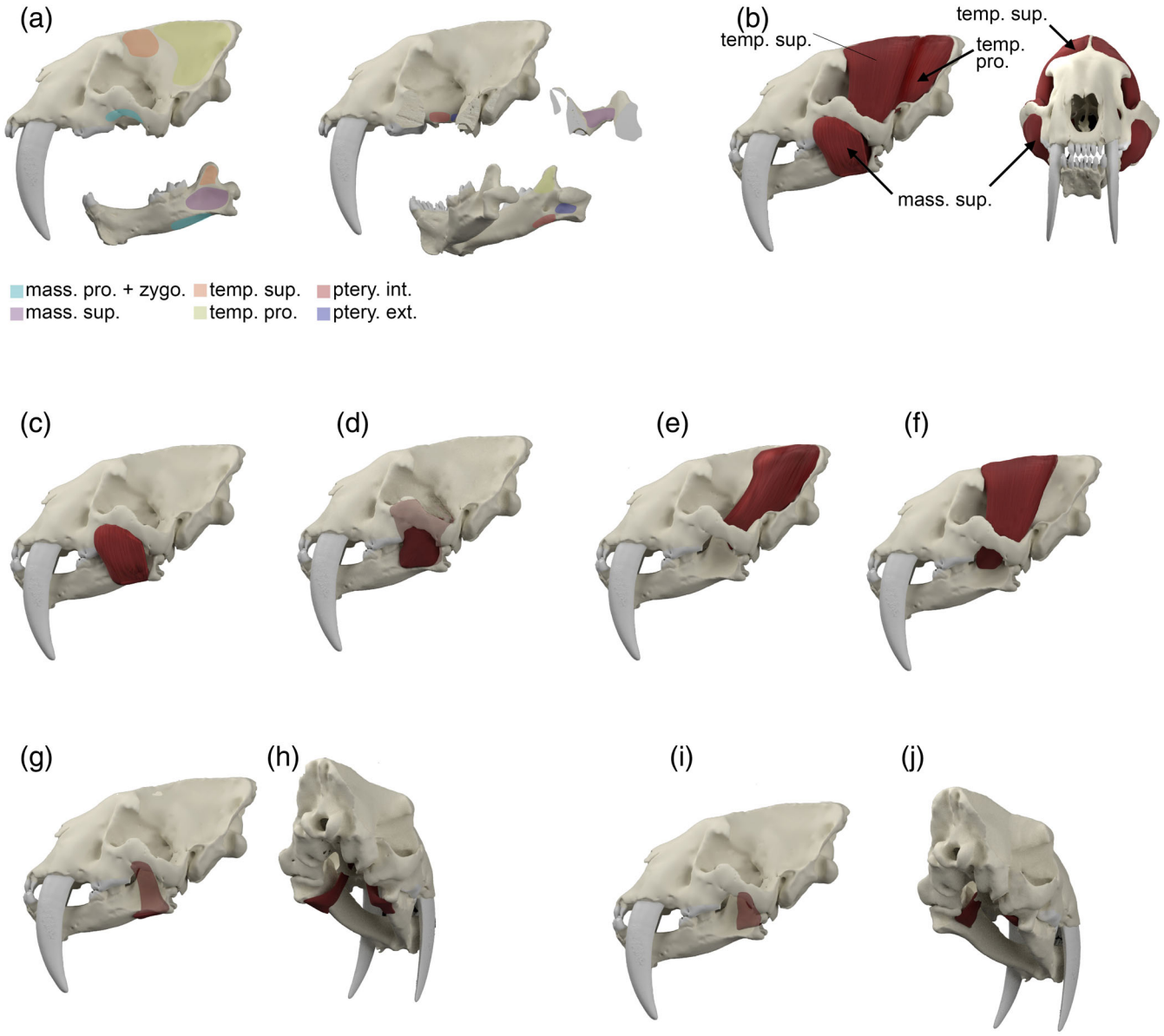

FIGURE 3 Origin and insertion areas for *S. fatalis* based on muscle scars and topological criteria for the three-dimensional muscle reconstruction. (a) Origin and insertion areas of main masticatory muscles reconstructed for intrinsic scenarios. (b) Reconstruction of tamporalis pars superficialis and pars profunda as well as the masseter pars superficialis. (c) The masseter pars superficialis. (d) Masseter pars profunda. (e) Temporalis pars profunda. (f) Temporalis pars superficialis. (g) and (h) Pterygoid pars interna in different views. (i) and (j) Pterygoid pars externa in different views. mass. pro., masseter pars profunda; mass. sup., masseter superficialis; temp. pro., temporalis pars profunda; temp. sup., temporalis pars superficialis; ptery. int., pterigoyd pars interna; ptery. ext., pterygoid pars externa.

of *B. fricki*, we modeled two different scenarios for the m. masseter pars profunda: (i) a traditional reconstruction, and (ii) a 'hystricomorph' configuration with the muscle extending into the infraorbital foramen as proposed by Naples and Martin (2000). This latter scenario was not performed on *S. fatalis* because the 'hystricomorph' arrangement of the masseter has been solely proposed for *B. fricki*. Due to the negligent effects of the pterygoideus muscles, these were omitted from the analyses.

2.4 | Finite element analysis

The 3D models of both skulls were imported into Hypermesh (version 11, Altair Engineering) for the generation of solid meshes (consisting of approximately 1,000,000 tetrahedral elements per model) and the setting of boundary conditions. Material properties for bone and teeth were assigned in Hypermesh (bone: $E = 13.7$ (cortical) GPa, $\upsilon = 0.30$, teeth: $E = 38.6.0$ GPa, $\upsilon = 0.4$) (Figueirido et al., 2018). All materials were treated as

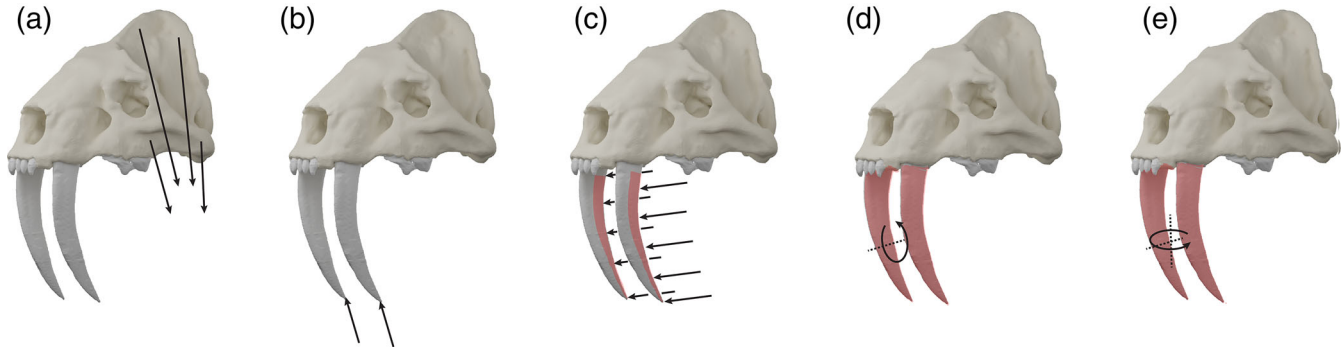

FIGURE 4 Simulated intrinsic and extrinsic scenarios of prey killing. (a) Jaw-adductor muscle-driven biting; (b) stabbing scenario; (c) pulling-back scenario; (d) lateral-shake scenario simulating torsional loads in *x*-direction; (e) lateral-shake scenario simulating torsional loads in *z*-direction. Black arrows indicate the direction of the forces applied (500 N on each canine). Red shaded area indicates degree to which the canines are simulated to be embedded in the prey (following Pollock et al., 2022).

isotropic and homogeneous. Bone and teeth were each assigned a single material property, as some of the CT data did not allow differentiating individual components (e.g., dentine, enamel).

We modeled two different intrinsic scenarios for unilateral and bilateral carnassial biting: (i) simulated a jaw adductor muscle-driven biting. Models in this scenario were constrained at the tip of the carnassial tooth (one node on each side) at the protocone to restrain the model from movement in *x*- and *y*-direction (i.e., medial/lateral and anterior/posterior), but not in *z*-direction to simulate some penetration of the teeth into the prey during biting. Additionally, we tested (ii) a further intrinsic scenario for *B. fricki* using the hystricomorph configuration of the masseter pars profunda.

We also tested three extrinsic scenarios of prey-killing, simulating the external forces supported by the skull when exerting the killing bite: (i) a stabbing scenario in which the saber-tooth stabs their prey using both canine teeth with a dorsally directed extrinsic force of 500 N applied to the tips of both canines (one node on each tooth) (Figure 4a), which makes in total 1000 N; (ii) a pulling-back scenario in which the predator pulls the head posteriorly with both canine teeth fully embedded in the prey and an extrinsic force of 500 N distributed over the posterior edge of the canines (10 nodes on each tooth) (Figure 4b); and (iii) a torsional scenario simulating the forces of struggling prey with both canines fully embedded in the prey. For this, we simulated torsional forces in two directions and an extrinsic force of 500 N applied to both canines (10 nodes on each side linked via a central proxy node to which the rotational forces were applied) (Figure 4c). We preferred to model torsional directions instead of a lateral force directly exerted on the canines sensu Figueirido et al. (2018) because it may reflect the shaking of the prey by the saber-tooth or struggling prey better than single-direction loads. The two directions were torsion perpendicular (along the *y*-axis) and parallel (along the *z*-axis) to the canines.

Therefore, the canine-shear bite should be considered as a combination of the stabbing and biting model scenarios, because it represents a two-step sequence that are not contemplated simultaneously in static FE analyses.

The extrinsic force (total of 1000 N for each scenario) was selected based on reported magnitudes for a neck-muscle-driven bite force (McHenry et al., 2007). For the extrinsic scenarios, the skull models of both species were scaled to the same surface area (of *Barbourofelis*, 171,825 mm^2) to remove functional artifacts due to size differences (Dumont et al., 2009). Constraints were placed on the articular surface of the squamosal (five nodes on each side), as well as the occipital condyle (10 nodes) to restrain the model from movement in *x*-, *y*-, and *z*-directions to simulate the fixed contact of the skull with other skeletal elements (i.e., mandible and vertebral column).

All models were imported into Abaqus (version 6.141, Simulia) for analysis and post-processing. Biomechanical performance for the FE models was assessed via contour plots of von Mises stress distribution, reaction forces, and ridgeline plots showing the stress distribution and frequency of stress magnitudes with the top 1% of values removed to avoid the influence of individual stress singularities at constrained or loaded nodes (Dumont et al., 2005).

3 | RESULTS

3.1 | Reaction force at the bite point and gape angle

The reaction force measured at different bite points for *S. fatalis* and for *B. fricki* under unilateral and bilateral carnassial biting scenarios, as well as the reaction forces at

TABLE 1 Reaction forces (in Newtons) at the bite point assuming a felid-like muscle arrangement for *S. fatalis* and *B. fricki*.

Taxa	Unilateral carnassial bite	Bilateral carnassial bite
S. fatalis	549	1066
B. fricki		
Felid-like muscle arrangement	655	1216
Hystricomorph muscle arrangement	717	1314

Note: The reaction forces obtained simulating an hystricomorph arrangement for the deep masseter of *B. fricki* are also shown.

the bite point simulating an 'hystricomorph' arrangement for the masseter pars profunda of *B. fricki* for unilateral and bilateral scenarios are shown in Table 1.

The analysis of the maximum gape angle based on muscle tension for the two different scenarios of the m. masseter pars profunda resulted in no meaningful differences. The traditional reconstruction allowed a gape angle of 73°, whereas the 'hystricomorph' reconstruction produced a slightly lower angle of 70.5° (Figure 5).

3.2 | Intrinsic scenarios

Contour plots of von Mises stress distributions for *S. fatalis* and *B. fricki* for unilateral and bilateral carnassial biting simulations (intrinsic scenarios of muscle-driven bite) are shown in Figure 6. Results show that there are no noteworthy differences in stress distribution and magnitude between both species of saber-tooths in both unilateral and bilateral scenarios. However, some slight differences appear between the unilateral and bilateral carnassial biting simulations in both species. Indeed, the ridgeline graphs depicted from the frequency of elements and the von Mises stress values confirm that the stress is distributed across the skull similarly in both species when simulating unilateral and bilateral carnassial biting scenarios (Figure 6). However, it is true that the skull of *B. fricki* appears to be less stressed than the one of *S. fatalis* when simulating bilateral canine biting. Despite this, during unilateral scenarios, the occipital region of *B. fricki* is more stressed than the same region of the skull of *S. fatalis*. The regions that are more stressed in both *S. fatalis* and *B. fricki* are the occipital bones, the zygomatic arches and, in *B. fricki*, the preorbital and postorbital bar (Figure 6).

The comparison of stress distribution across the skull of *B. fricki* obtained from the simulation with a conventional masseter arrangement and from the simulation with an hystricomorph arrangement of the masseter pars profunda indicate no substantial differences between both scenarios. However, the postorbital bar seems to be slightly less stressed with a hystricomorph arrangement (Figure 6). The ridgeline plots also show a very similar distribution of the frequency of elements with a given value of von Mises stress for both scenarios.

3.3 | Extrinsic scenarios

Contour plots of von Mises stress distributions for *S. fatalis* and *B. fricki* for stab, pull-back, and torsional simulations are shown in Figure 7.

For the stabbing scenario, the stresses in *S. fatalis* are evenly distributed across the skull but the regions with pronounced stresses are the zygomatic arch, the maxilla, and in the posterior part of the frontal bone (Figure 7a). In contrast, the stresses in the skull of *B. fricki* are not as evenly distributed as in the skull of *S. fatalis*, and the regional stress is mainly present in the occipital and parietal bones, as well as in the upper canines (Figure 7a).

In the case of the pulling-back scenario, the stresses are more evenly distributed across the skull of *S. fatalis* than across the skull of *B. fricki* but the zygomatic, the posterior part of the frontal bone and, to a lesser degree, the maxilla present high stresses (Figure 7b). In *B. fricki*, the stresses seem to be concentrated in the premaxilla, the occipitals and, again, in the canines (Figure 7b).

Strikingly, the torsional scenario in *y*-direction clearly differentiates the stress distribution across the skull in both saber-tooths (Figure 7c). The skull of *S. fatalis* is highly stressed almost entirely, except for the premaxilla and the occipital bone, but the stress distribution across the skull of *B. fricki* is solely concentrated across the premaxilla, the parietal-occipital region, the postorbital bar, and across the canines (Figure 7c).

The results obtained for the torsional scenario in *z*-direction indicate that the stresses are mainly concentrated across the rostrum of both taxa (Figure 7d). However, the skull of *S. fatalis* exhibits much more stress than the one of *B. fricki*, particularly across the zygomatic, the posterior region of the frontal bone and, in a lesser degree, across the nasals (Figure 7d).

4 | DISCUSSION

In this study, we have CT-scanned the skull of *B. fricki* for the first time and we have compared its cranial mechanics to the skull of *S. fatalis*, two species of dirk-toothed sabertooths from the Miocene and Pleistocene of North America, respectively. Our main goal was to

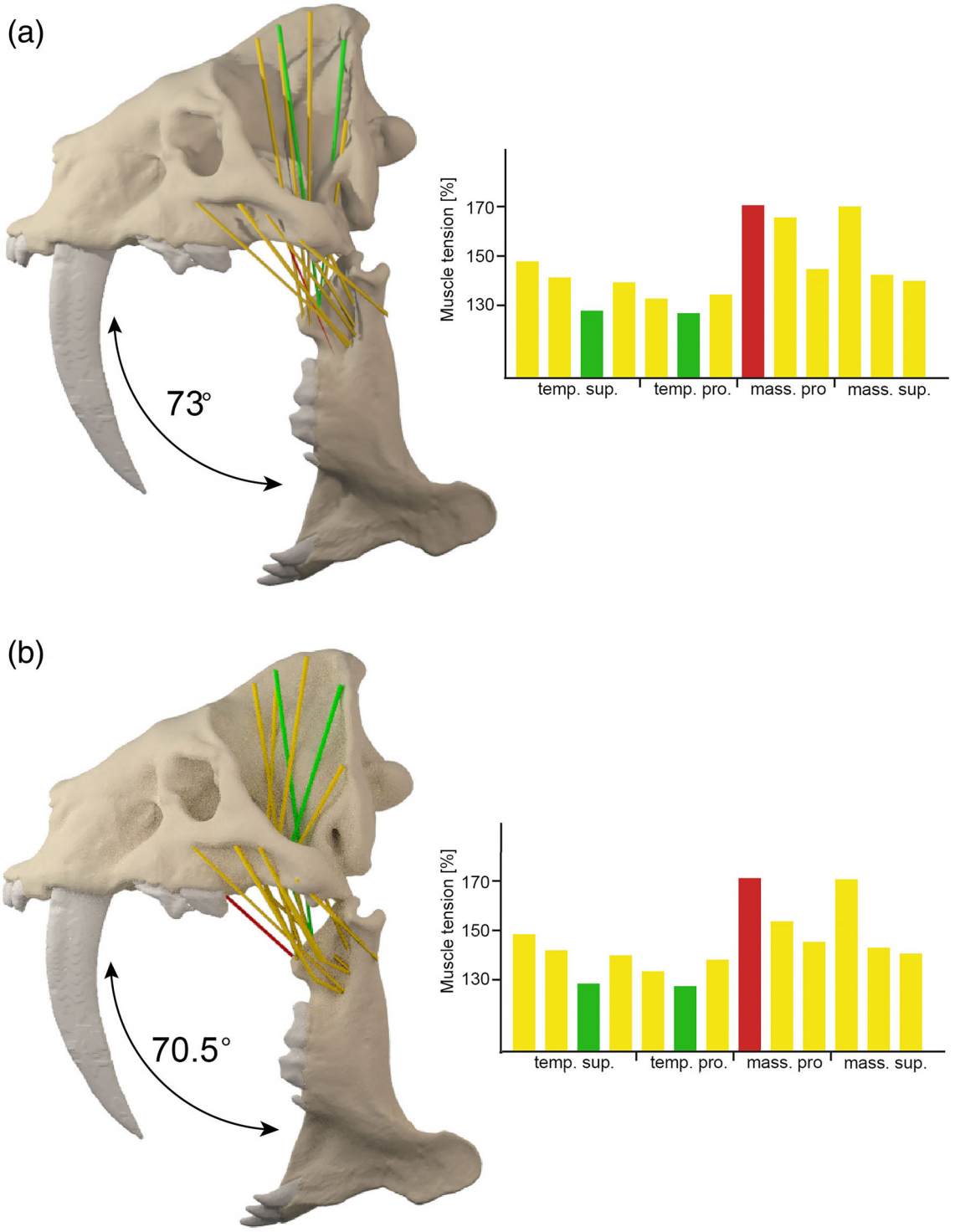

FIGURE 5 Muscle-constrained gape angle analyses comparing different configurations for the m. masseter pars profunda. (a) Traditional reconstruction, (b) 'hystricomorph' as proposed by Naples and Martin (2000). Muscle tension at maximum gape angle are shown for each adductor muscle in the respective bar charts. temp. pro., temporalis pars profunda; temp. sup., temporalis pars superficialis; mass. pro., masseter pars profunda; mass. sup., masseter pars superficialis.

investigate potential differences in killing behavior among species belonging to the same ecomorph of saber-tooths. Furthermore, our study provides new insights into the cranial biomechanics of *B. fricki*, a understudied species with more advanced saber-tooth characteristics than *S. fatalis*.

Our results show that for the intrinsic muscle-driven scenarios, the skull of *B. fricki* behaves similarly to the

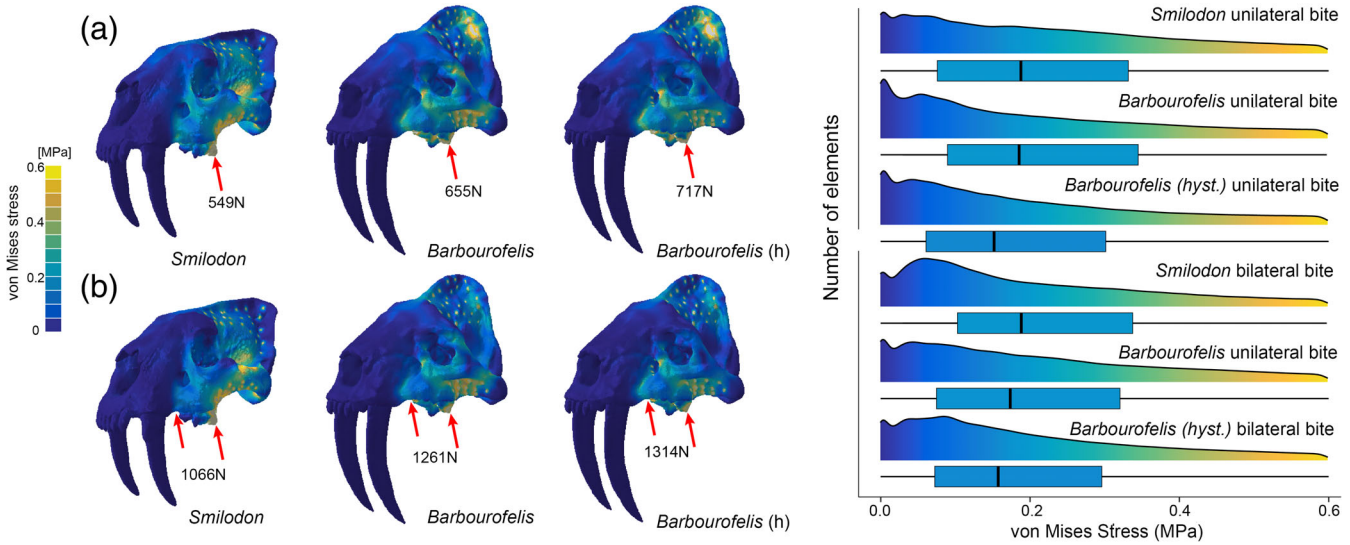

FIGURE 6 von Mises stress (MPa) contour plots obtained from finite element analysis of the crania of *B. fricki* and *S. fatalis* after the simulation of intrinsic scenarios. (a) Unilateral carnassial biting. (b) Bilateral carnassial biting. Red arrows indicate the direction of the exerted force. Ridgeline showing the distribution of the percentage of the element frequency (*y*-axis) to a given value of von Mises stress (*x*-axis) are shown for unilateral and bilateral carnassial biting. The box-plots represent the von Mises stress values for each scenario. Central bar indicates the mean value, top and bottom of box indicate the 25% and 75% quartiles, whiskers indicate maximum and minimum values. The results for *B. fricki* and *S. fatalis* are obtained from the conventional arrangement of the deep masseter, while the result of *B. fricki* (hyst.) is obtained from the hystricomorph arrangement of this muscle, following Naples and Martin (2000).

one of *S. fatalis* in terms of von Mises stress distribution and reaction forces on the bite point (as a proxy for bite forces). This difference in reaction forces is surprising, as the skull of *B. fricki* is ca. 15% smaller. Moreover, the simulations performed with an hystricomorph arrangement of the masseter—that is, when the masseter pars profunda originated from the maxilla through the infraorbital foramen to be inserted in the masseteric fossa, show no substantial differences in gape angle, reaction forces, and stress dissipation than the simulations performed with a conventional masseter arrangement. Therefore, our data suggest that there is no biomechanical reason to support hystricomorphy as an adaptation to facilitate jaw closure from gapes over 90° (Naples & Martin, 2000).

Strikingly, our results also show that for all extrinsic scenarios (i.e., stab, pull-back, torsion) the skulls of *B. fricki* and *S. fatalis*, despite being both dirk-toothed saber-tooths, possess different cranial mechanics. In general terms, the skull of *B. fricki* is very stress-resistant compared to the skull of *S. fatalis* in absolute values. Indeed, in all extrinsic scenarios, while the stress is more evenly distributed in the skull of *S. fatalis*, more elements experience high stresses. Conversely, in *B. fricki* more elements experience low stresses, which means that there are only regional stress hotspots in *B. fricki*, but nearly the entire skull is affected in *S. fatalis*. This is likely related to an optimized stress dissipation in *B. fricki*, with stress hotspots limited mostly to the premaxilla and maxilla, and to a lesser degree the parietal and postorbital bar, whereas stresses are distributed over the entire skull in *S. fatalis*.

Despite the very stress-resistant skull configuration of *B. fricki*, its canines are very weak when extrinsic forces are applied. The canines of *B. fricki* are longer and exhibit a higher degree of mediolateral compression (Bryant, 1990) than the ones of *S. fatalis* (Figure 1). Physical testing of pointed teeth shows that sharp and slender forms decrease puncture force in ductile materials (Evans & Sanson, 1998; Freeman & Lemen, 2006; Pollock et al., 2024) and, therefore, the sharp upper canines of *B. fricki* most probably penetrated prey skin more easily, something that is not entirely reflected in our finite element models. Therefore, stresses generated in the canines would be transferred to a certain amount to the stoutly built skull of *B. fricki*, being able to support such stresses.

B. fricki is characterized by the presence of a postorbital bar, a trait that is also shared with the South American sparassodont *T. atrox*. Moreover, both dirk-tooths also exhibit a genial mandibular flange, a trait not shared with *S. fatalis* (Figure 1). Much has been discussed about the function of the postorbital bar in mammals (e.g., Greaves, 1985; Heesy, 2005; Noble et al., 2000). However, the most accepted hypothesis is that it stiffens the lateral orbital wall in taxa that have significant angular deviation between the temporal fossa and the bony

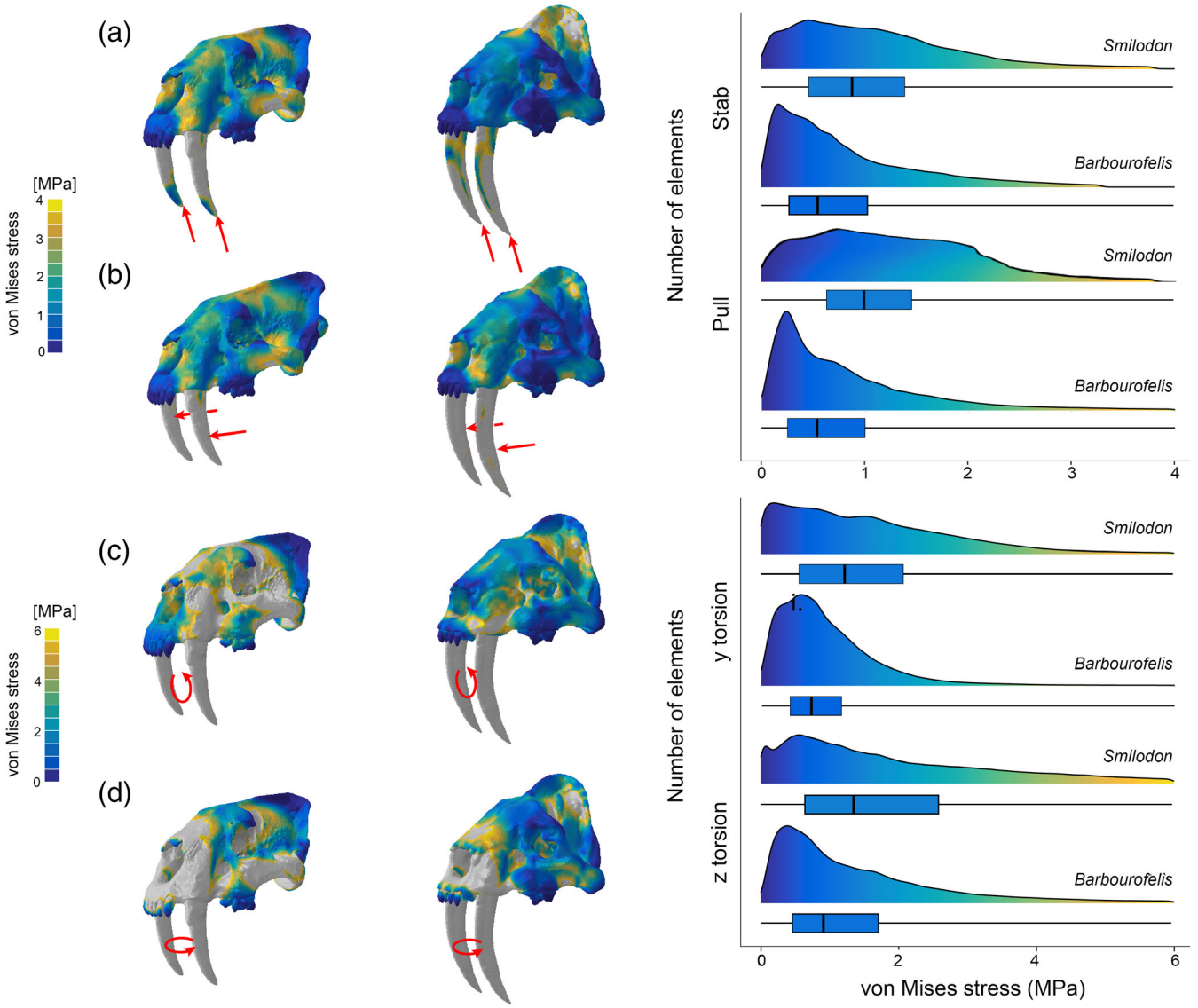

FIGURE 7 von Mises stress (MPa) contour plots obtained from finite element analysis of the crania of *B. fricki* and *S. fatalis* after the simulation of extrinsic scenarios. (a) Stab. (b) Pull-back. (c) Torsion in *y*-direction. (d) Torsion in *z*-direction. Ridgeline showing the distribution of the percentage of the element frequency (*y*-axis) to a given value of von Mises stress (*x*-axis) are shown for unilateral and bilateral canine biting. The box-plots represent the von Mises stress values for each scenario. Central bar indicates the mean value, top and bottom of box indicate the 25% and 75% quartiles, whiskers indicate maximum and minimum values.

orbit to avoid deformation of the soft tissues due to the temporalis contraction and assuring normal oculomotor function (Heesy, 2005). Our results suggest that the post-orbital bar is not particularly a region of stress concentration when simulating intrinsic and extrinsic scenarios, except in the case of the torsional scenario perpendicular to canines (Figure 7c).

While there have been observations of morphological differences among the different ecomorphs of saber-tooths (dirk and scimitar), it has commonly been assumed that they all used the same killing behavior to dispatch their prey (e.g., Christiansen, 2007; Emerson & Radinsky, 1980; Figueirido et al., 2011). The prevailing hypothesis regarding the killing behavior of dirk and scimitar saber-tooths has been the canine-shear bite proposed by Akersten (1985). However, recent biomechanical evidence suggests that dirk and scimitar forms use different killing strategies to dispatch their prey (Figueirido et al., 2018). Moreover, a recent study (Janis et al., 2020) suggests that *T. atrox* may have been scavenging the internal organs of prey previously predated by other South American faunal elements (but see Melchionna et al., 2021; Wroe et al., 2013). If the hypothesis of Janis et al. (2020) holds true, this implies that

T. atrox might not have used a canine-shear bite to dispatch its prey with its divergent canines.

Our results suggest that the skull of *B. fricki* experienced comparatively lower stresses in all simulated prey-killing scenarios relative to *S. fatalis*, the latter experiencing lower stresses only in a stabbing scenario. This may indicate that *B. fricki* was more generalist in prey-killing than *S. fatalis*, a hypothesis that seems, a priori, counterintuitive, because the skull of *B. fricki* is much more specialized in terms of morphology towards the saber-tooth ecomorph than the one of *S. fatalis*—that is, a more verticalized temporal fossa, shorter coronoids, longer and narrower upper canines (Figure 1). However, in our view, morphological specialization is decoupled from ecological specialization in saber-tooths, because specialization in morphology depends on the length of the canine (Meloro & Slater, 2012; Slater & Van Valkenburgh, 2008). Therefore, our findings support the notion proposed by Lautenschlager et al. (2020) and Chatar et al. (2022) in which morphological convergence among saber-tooths may obscure functional diversity and thereby differences in their killing behavior.

In any case, our results indicate potential differences in prey-killing among species within the same ecomorph, which cast doubts about whether the canine-shear bite can be universally assumed as the predatory behavior of all saber-tooths. Although our analyses were conducted on only two species and might not represent the general pattern for all dirk-tooths, our results support potential differences in predatory behavior between *B. fricki* and *S. fatalis*. Given that previous studies document profound interspecific differences in morphology among saber-tooths (e.g., Emerson & Radinsky, 1980; Slater & Van Valkenburgh, 2008), future research involving a wider range of dirk-toothed species, as well as other species of scimitar forms, could offer further insights into the diversity of cranial biomechanics within this intriguing group of extinct mammalian predators.

AUTHOR CONTRIBUTIONS

Borja Figueirido: Conceptualization; writing – original draft; project administration; investigation; writing – review and editing. **Shane Tucker:** Data curation. **Stephan Lautenschlager:** Investigation; conceptualization; writing – original draft; methodology; formal analysis; writing – review and editing.

ACKNOWLEDGMENTS

We are very grateful to Adam Harstone-Rose, Tahlia Pollock and Lars Werdelin for organizing the symposium of sabertooth biology at the ICVM 2023 and for inviting us to present our work. Chrisitine Janis provided comments on an early version of this manuscript. We are also grateful to Georgia Blobaum at Advanced Medical Imaging for providing access to CT-scans and to the Digimorph team, especially Jessie Maisano, for kindly providing the CT of *S. fatalis* analyzed in this study. We are especially grateful to Ross Secord for kindly providing access to the skull of *B. fricki*. We are gateful to two anonymous reviewers who greatly improved the clarity and rigor of the manuscript.

FUNDING INFORMATION

This study has been funded by the Ministerio de Economía y Competitividad (grant numbers CGL2015-68300P and PID2019-111185GB-I00) and Junta de Andalucía (P18-FR-3193; UMA18-FEDERJA-188) to BF Funding for open acess; University of Málaga/CBUA.

CONFLICT OF INTEREST STATEMENT

The authors declare that there are not conflict of interest.

DATA AVAILABILITY STATEMENT

The data of *B. fricki* is available on figshare

ORCID

Borja Figueirido https://orcid.org/0000-0003-2542-3977

REFERENCES

Akersten, W. (1985). Canine function in *Smilodon* (Mammalia, Felidae, Machairodontinae). *Natural History Museum of Los Angeles County, Contributions in Science*, *356*, 1–22.

Andersson, K., Norman, D., & Werdelin, L. (2011). Sabretoothed carnivores and the killing of large prey. *PLoS One*, *6*(10), e24971.

Antón, M., & Galobart, À. (1999). Neck function and predatory behavior in the scimitar toothed cat *Homotherium latidens* (Owen). *Journal of Vertebrate Paleontology*, *19*(4), 771–784. https://doi.org/10.1080/02724634.1999.10011190

Antón, M., Salesa, M. J., Pastor, J. F., Sánchez, I. M., Fraile, S., & Morales, J. (2004). Implications of the mastoid anatomy of larger extant felids for the evolution and predatory behaviour of sabretoothed cats (Mammalia, Carnivora, Felidae). *Zoological Journal of the Linnean Society*, *140*, 207–221.

Ballesio, R. (1963). Monographie d'un Machairodus du gisement villafranchien de Senéze: *Homotherium crenatidens* Fabrini. *Traveaux du Laboratoire de Géologie de la Faculte de Sciences de Lyon*, *9*, 1–129.

Barrett, P. Z. (2021). The largest hoplophonine and a complex new hypothesis of nimravid evolution. *Scientific Reports*, *11*(1), 21078.

Barrett, P. Z., Hopkins, S. S., & Price, S. A. (2021). How many sabertooths? Reevaluating the number of carnivoran sabretooth lineages with total-evidence Bayesian techniques and a novel origin of the Miocene Nimravidae. *Journal of Vertebrate Paleontology*, *41*(1), e1923523.

Bohlin, B. (1940). Food habit of the Machaerodonts, with special regard to *Smilodon*. *Bulletin of the Geological Institutions of the University of Uppsala*, *28*, 156–174.

Brown, J. G. (2014). Jaw function in *Smilodon fatalis*: A reevaluation of the canine shear-bite and a proposal for a new forelimb-powered class 1 lever model. *PLoS One*, *9*(10), e107456.

Bryant, H. N. (1990). Implications of the dental eruption sequence in *Barbourofelis* (Carnivora, Nimravidae) for the function of upper canines and the duration of parental care in sabretoothed carnivores. *Journal of Zoology*, *222*(4), 585–590.

Bryant, H. N. (1996). Force generation by the jaw adductor musculature at different gapes in the Pleistocene sabretoothed felid *Smilodon*. In K. M. Stewart & K. L. Seymour (Eds.), *Paleoecology and paleoenvironments of late Cenozoic mammals* (pp. 283–299). University of Toronto Press.

Chatar, N., Fischer, V., & Tseng, Z. J. (2022). Many-to-one function of cat-like mandibles highlights a continuum of sabre-tooth adaptations. *Proceedings of the Royal Society B*, *289*(1988), 20221627.

Christiansen, P. (2007). Comparative bite forces and canine bending strength in feline and sabretooth felids: Implications for predatory ecology. *Zoological Journal of the Linnean Society*, *151*(2), 423–437.

Dumont, E. R., Grosse, I. R., & Slater, G. J. (2009). Requirements for comparing the performance of finite element models of biological structures. *Journal of Theoretical Biology*, *256*(1), 96–103.

Dumont, E. R., Piccirillo, J., & Grosse, I. R. (2005). Finite-element analysis of biting behavior and bone stress in the facial skeletons of bats. *The Anatomical Record. Part A, Discoveries in Molecular, Cellular, and Evolutionary Biology*, *283*, 319–330.

Emerson, S. B., & Radinsky, L. (1980). Functional analysis of sabertooth cranial morphology. *Paleobiology*, *6*, 295–312.

Evans, A. R., & Sanson, G. D. (1998). The effect of tooth shape on the breakdown of insects. *Journal of Zoology*, *246*(4), 391–400.

Faith, J. T., Rowan, J., Du, A., & Koch, P. L. (2018). Plio-Pleistocene decline of African megaherbivores: No evidence for ancient hominin impacts. *Science*, *362*(6417), 938–941.

Figueirido, B., Lautenschlager, S., Pérez-Ramos, A., & Van Valkenburgh, B. (2018). Distinct predatory behaviors in scimitar- and dirk-toothed sabertooth cats. *Current Biology*, *28*(20), 3260–3266.

Figueirido, B., MacLeod, N., Krieger, J., De Renzi, M., Pérez-Claros, J. A., & Palmqvist, P. (2011). Constraint and adaptation in the evolution of carnivoran skull shape. *Paleobiology*, *37*(3), 490–518.

Freeman, P. W., & Lemen, C. (2006). Puncturing ability of idealized canine teeth: Edged and non-edged shanks. *Journal of Zoology*, *269*(1), 51–56.

Gaillard, C., MacPhee, R. D., & Forasiepi, A. M. (2023). Seeing through the eyes of the sabertooth *Thylacosmilus atrox* (Metatheria, Sparassodonta). *Communications Biology*, *6*(1), 257.

Greaves, W. S. (1985). The mammalian postorbital bar as a torsion-resisting helical strut. *Journal of Zoology*, *207*(1), 125–136.

Heesy, C. P. (2005). Function of the mammalian postorbital bar. *Journal of Morphology*, *264*(3), 363–380.

Herbst, E. C., Meade, L. E., Lautenschlager, S., Fioritti, N., & Scheyer, T. M. (2022). A toolbox for the retrodeformation and muscle reconstruction of fossil specimens in Blender. *Royal Society Open Science*, *9*(8), 220519.

Janis, C. M., Figueirido, B., DeSantis, L., & Lautenschlager, S. (2020). An eye for a tooth: *Thylacosmilus* was not a marsupial "saber-tooth predator". *PeerJ*, *8*, e9346.

Kurtén, B. (1952). The Chinese hipparion fauna. *Commentationes Biologicae (Societas Scientarum Fennica).*, *13*, 1–82.

Lautenschlager, S. (2013). Cranialmyology and bite force performance of E rlikosaurus andrewsi: a novel approachfor digital muscle reconstructions. *Journal of Anatomy*, *222*(2), 260–272.

Lautenschlager, S. (2015). Estimating cranial musculoskeletal constraints in theropod dinosaurs. *Royal Society Open Science*, *2*, 150495.

Lautenschlager, S. (2016). Reconstructing the past: Methods and techniques for the digital restoration of fossils. *Royal Society Open Science*, *3*(10), 160342.

Lautenschlager, S., Figueirido, B., Cashmore, D. D., Bendel, E. M., & Stubbs, T. L. (2020). Morphological convergence obscures functional diversity in sabre-toothed carnivores. *Proceedings of the Royal Society B*, *287*(1935), 20201818.

Martin, L. D. (1980). Functional morphology and the evolution of cats. *Transactions of the Nebraska Academy of Sciences and Affiliated Societies*, *287*, 141–154.

Matthew, W. D. (1910). The phylogeny of the Felidae. *Bulletin of the American Museum of Natural History*, *28*, 289–318.

McHenry, C. R., Wroe, S., Clausen, P. D., Moreno, K., & Cunningham, E. (2007). Supermodeled sabercat, predatory behavior in *Smilodon fatalis* revealed by high-resolution 3D computer simulation. *Proceedings of the National Academy of Sciences*, *104*(41), 16010–16015.

Melchionna, M., Profico, A., Castiglione, S., Serio, C., Mondanaro, A., Modafferi, M., Raia, P., & Sansalone, G. (2021). A method for mapping morphological convergence on three-dimensional digital models: the case of the mammalian sabre-tooth. *Palaeontology*, *64*(4), 573–584.

Meloro, C., & Slater, G. J. (2012).Covariation in the skull modules of cats: the challenge of growing saber-likecanines. *Journal of Vertebrate Paleontology*, *32*(3), 677–685.

Naples, V. L., & Martin, L. D. (2000). Evolution of hystricomorphy in the Nimravidae (Carnivora; Barbourofelinae): Evidence for complex character convergence with rodents. *Historical Biology*, *14*(3), 169–188.

Nigg, B. M., & Herzog, W. (2007). *Biomechanics of the musculoskeletal system*. Wiley.

Noble, V. E., Kowalski, E. M., & Ravosa, M. J. (2000). Orbit orientation and the function of the mammalian postorbital bar. *Journal of Zoology*, *250*(3), 405–418.

Piras, P., Maiorino, L., Teresi, L., Meloro, C., Lucci, F., Kotsakis, T., & Raia, P. (2013). Bite of the cats: Relationships between functional integration and mechanical performance as revealed by mandible geometry. *Systematic Biology*, *62*(6), 878–900.

Pollock, T. I., Hocking, D. P., & Evans, A. R. (2024). Is a blunt sword pointless? Tooth wear impacts puncture performance in Tasmanian devil canines. *Journal of Experimental Biology*, *227*(3), jeb246925.

Pollock, T. I., Panagiotopoulou, O., Hocking, D. P., & Evans, A. R. (2022). Taking a stab at modelling canine tooth biomechanics in mammalian carnivores with beam theory and finite-element analysis. *Royal Society Open Science*, *9*(10), 220701.

Schaub, S. (1925). Uber die Osteologie von *Machaerodus cultridens* Cuvier. *Eclogae Géologica Helvetiae*, *19*, 255–266.

Sherwood, L., Klandorf, H., & Yancey, P. (2012). *Animal physiology: From genes to organisms* (pp. 335–384). Brooks Cole.

Simpson, G. G. (1941). The function of saber-like canines in carnivorous mammals. *American Museum Novitates*, *1130*, 1–12.

Slater, G. J., & Van Valkenburgh, B. (2008). Long in the tooth: Evolution of sabertooth cat cranial shape. *Paleobiology*, *34*(3), 403–419.

Therrien, F. (2005). Feeding behaviour and bite force of sabretoothed predators. *Zoological Journal of the Linnean Society*, *145*(3), 393–426.

Thomason, J. J. (1991). Cranial strength in relation to estimated biting forces in some mammals. *Canadian Journal of Zoology*, *69*, 2326–2333.

Turner, A., Antón, M., Salesa, M. J.,& Morales, J. (2011). Changing ideas about the evolution and functionalmorphology of Machairodontine felids. *Estudios Geológicos*, *67*(2), 255–276.

Van Valkenburgh, B. (2007). Déjà vu: theevolution of feeding morphologies in the Carnivora. *Integrative and comparative biology*, *47*(1), 147–163.

Van Valkenburgh, B., Hayward, M. W., Ripple, W. J., Meloro, C., & Roth, V. L. (2016). The impact of large terrestrial carnivores on Pleistocene ecosystems. *Proceedings of the National Academy of Sciences*, *113*(4), 862–867.

Wang, X., White, S. C., & Guan, J. (2020). A new genus and species of sabretooth, *Oriensmilus liupanensis* (Barbourofelinae, Nimravidae, Carnivora), from the middle Miocene of China suggests barbourofelines are nimravids, not felids. *Journal of Systematic Palaeontology*, *18*(9), 783–803.

Wroe, S., Chamoli, U., Parr, W. C., Clausen, P., Ridgely, R., & Witmer, L. (2013). Comparative biomechanical modeling of metatherian and placental saber-tooths: A different kind of bite for an extreme pouched predator. *PLoS One*, *8*(6), e66888.

How to cite this article: Figueirido, B., Tucker, S., & Lautenschlager, S. (2024). Comparing cranial biomechanics between *Barbourofelis fricki* and *Smilodon fatalis*: Is there a universal killing-bite among saber-toothed predators? *The Anatomical Record*, 1–14. https://doi.org/10.1002/ar.25451